Structural variations and dielectric properties of $(Bi_{1-x}La_x)_2SiO_5$ ($0 \leqslant x \leqslant 0.1$): Polycrystallines synthesized by crystallization of Bi-Si-O and Bi-La-Si-O glasses

Hiroki Taniguchi,[1,4,*] Shingo Tatewaki,[1] Shintaro Yasui,[2] Yasuhiro Fujii,[3] Jun-ichi Yamaura,[4] and Ichiro Terasaki[1]

[1]*Department of Physics, Nagoya University, Nagoya 464-8602, Japan*

[2]*Laboratory for Materials and Structures, Tokyo Institute of Technology, Yokohama, Kanagawa 226-8503, Japan*

[3]*Department of Physical Sciences, Ritsumeikan University, Kusatsu 525-8577, Japan*

[4]*Materials Research Center for Element Strategy, Tokyo Institute of Technology, Yokohama, Kanagawa 226-8503, Japan*

(Received 10 January 2018; published 17 April 2018)

This paper focuses on effects of isovalent La substitution on the crystal structure and dielectric properties of ferroelectric Bi_2SiO_5. Polycrystalline samples of $(Bi_{1-x}La_x)_2SiO_5$ are synthesized by crystallization of Bi-Si-O and Bi-La-Si-O glasses with a composition range of $0 \leqslant x \leqslant 0.1$. The crystal structure changes from monoclinic to tetragonal with increasing La-substitution rate x at room temperature. This structural variation stems from the change in orientation of SiO_4 tetrahedra that form one-dimensional chains when they are in the ordered configuration, thus suggesting that lone-pair electrons play an important role in sustaining one-dimensional chains of SiO_4 tetrahedra. Synchronizing with the disordering of SiO_4 chains, ferroelectric phase transition temperature of $(Bi_{1-x}La_x)_2SiO_5$ sharply decreases as x increases, and ferroelectricity finally vanishes at around $x = 0.03$. The present results demonstrate that lone-pair electrons of Bi play an important role in the ferroelectricity of Bi_2SiO_5 through propping the ordered structure of one-dimensional SiO_4 chains with stereochemical activity. Furthermore, an additional phase transition has been first discovered in the low-temperature region of $(Bi_{1-x}La_x)_2SiO_5$ with $x \leqslant 0.01$, where the ordered one-dimensional SiO_4 chains remain.

DOI: 10.1103/PhysRevMaterials.2.045603

I. INTRODUCTION

Lately, much effort has been devoted to clarifying the key factors in ferroelectricity design, since new ferroelectric materials contribute to the fundamental understanding of phase transitions and critical phenomena, as well as to the development of novel functional devices such as high-density capacitors, nonvolatile memories, and the like [1,2]. The most common family of ferroelectrics is a group of perovskite-type oxides with ABO_3 stoichiometry represented by $BaTiO_3$, $Pb(Zr,Ti)O_3$, and $BiFeO_3$. These perovskite-type oxides incorporate BO_6 oxygen octahedra in their crystal structure; interactions among the B-site cation and the neighboring oxygen anions often give rise to non-centro-symmetric deformation of the BO_6 octahedron, thus inducing ferroelectricity [3–9]. An A-site cation with lone-pair electrons may show strong polar displacement against BO_6 octahedra, as a stereochemical effect [10,11]. A special combination of ionic sizes for A- and B-site cations results in a delicate balance between their ferroelectric interaction and fluctuations to violate polar ordering, leading to quantum para(ferro)electricity [12–15]. The phase transition is broadened, allowing for large permittivity over a wide temperature range, as the cations compete for charge neutrality and ionic size matching [16–19]. Recently, the rational design of oxygen-octahedra-based ferroelectric oxides has remarkably improved due to the development of first-principles calculations [20–22].

Although, compared to octahedra-based oxides, new ferroelectric materials with oxygen-tetrahedra have been underdeveloped, a unique ferroelectricity mechanism was recently reported in Bi_2SiO_5, which is composed of one-dimensional chains of SiO_4 tetrahedra [23–25]. In contrast to octahedra-based ferroelectrics, where ferroelectricity stems from relative displacements of oxygen octahedra and cations, Bi_2SiO_5 ferroelectricity is induced by zig-zag tilting of SiO_4 chains [23,26]. Along with the tilting of SiO_4 tetrahedra, internal deformation of SiO_4 tetrahedra takes place to produce large spontaneous polarization comparable to that of $BaTiO_3$. A ferroelectric phase transition of Bi_2SiO_5 from a paraelectric phase of orthorhombic $Cmcm$ symmetry to a ferroelectric phase of monoclinic Cc symmetry occurs at a rather high temperature around 400 °C on cooling. Such excellent properties found in Bi_2SiO_5 indicate great potential of tetrahedra-based oxides for the development of ferroelectric materials with excellent functionalities. Other examples of functional ferroelectric oxides with oxygen tetrahedra can be found in a family of stuffed zeolites, some of which show an excellent performance for pyroelectric energy harvesting due to their improper ferroelectricity [27–29].

Figure 1 depicts the crystal structure of Bi_2SiO_5 in comparison with perovskite-type, aurivillius-type, and brownmillerite-type structures. The aurivillius-type structure is obtained by replacing one in every two octahedral layers of the perovskite-type structure with a fluorite-type Bi_2O_2 layer, whereas the brownmillerite-type structure is given by alternatively substituting parallel-aligned one-dimensional tetrahedral chains for octahedral layers. Additionally, the crystal structure of Bi_2SiO_5 can be obtained when the perovskite-type structure is

*Corresponding author: hiroki_taniguchi@cc.nagoya-u.ac.jp

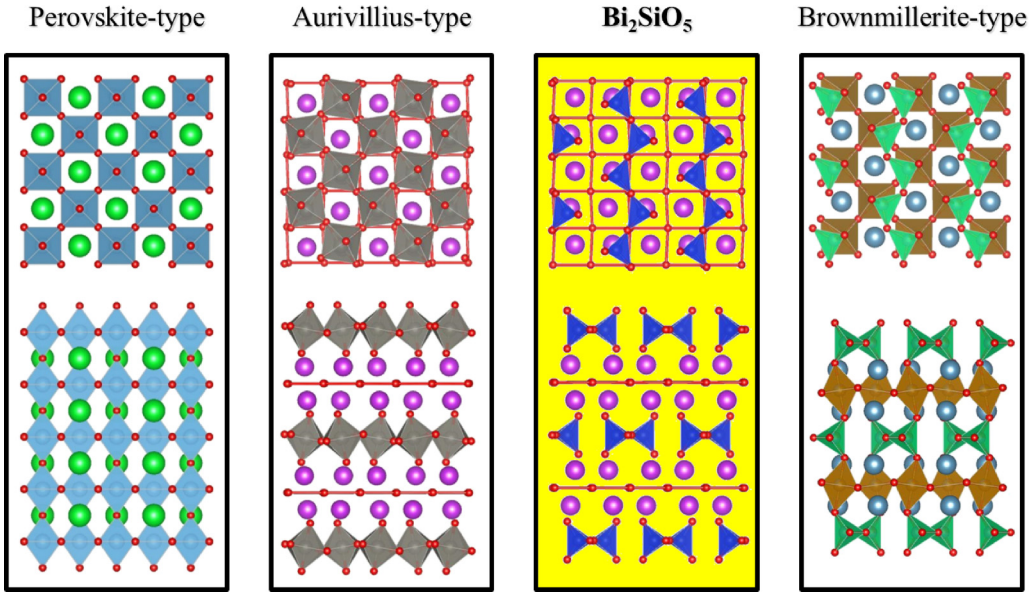

FIG. 1. A comparison of perovskite-type, aurivillius-type, and brownmillerlite-type crystal structures with that of Bi_2SiO_5. The crystal structure of Bi_2SiO_5 can be understood by successive replacement of one in every two octahedral layers by fluorite-type Bi_2O_2 layers and parallel-aligned one-dimensional tetrahedral chains, which are involved in the aurivillius-type and brownmillerlite-type crystal structures, respectively. (See text for details.)

subjected to both replacements applied to the aurivillius- and brownmillerite-type structures. Such a crystallographic link implies diversity in the choice of elements for substitution to design the physical properties of Bi_2SiO_5. A previous study on $(Bi_{1-x}Pb_x)_2SiO_{5-\delta}$ clarified that the ferroelectricity of Bi_2SiO_5 is tolerant to a large amount of oxygen vacancies introduced by heterovalent Pb^{2+} substitution up to $x = 0.2$ and proposed that lone-pair electrons in the Bi-site cation play a role in the ferroelectricity of Bi_2SiO_5.

Here, we perform isovalent substitution of La^{3+} to the Bi site of Bi_2SiO_5 to clarify the role of lone-pair electrons in the ferroelectricity of Bi_2SiO_5. Systematic studies with x-ray-diffraction measurements, Raman-scattering spectroscopy, and dielectric measurements on $(Bi_{1-x}La_x)_2SiO_5$ polycrystallines as a function of x have clarified that La substitution gives rise to disordering of the SiO_4-tetrahedral chains to strongly suppress the ferroelectricity of Bi_2SiO_5. Additional anomalies have been found in temperature dependences of lattice parameters and dielectric response in a low-temperature region of $(Bi_{1-x}La_x)_2SiO_5$ with $x \leqslant 0.01$, suggesting existence of an unknown ground state of Bi_2SiO_5.

II. EXPERIMENTAL

As Bi_2SiO_5 is metastable and exists only in a nonequilibrium phase diagram, polycrystalline samples of $(Bi_{1-x}La_x)_2SiO_5$ were fabricated with crystallization of Bi-Si-O and Bi-La-Si-O glasses, which were preliminarily synthesized by rapid quenching of stoichiometric melts [30]. For the crystallization, Bi-Si-O and Bi-La-Si-O glass samples were annealed at 600 ° C for 12 h to crystallize $(Bi_{1-x}La_x)_2SiO_5$ ($x = 0.00$, 0.01, 0.03, 0.05, 0.07, and 0.10). The annealing temperature was determined by *in situ* x-ray-diffraction measurements during the crystallization process of Bi_2SiO_5 using a four-axis diffractometer (Smartlab, Rigaku Co.) with a temperature-controlled chamber (DHS1100, Anton Paar). Details are provided in the following section. Powder x-ray-diffraction patterns of the obtained samples were measured with grinded powders for each composition at room temperature by RIGAKU RINT-2200. The Cu-Kα line with the wavelength of 1.5405 Å was used as the incident for all x-ray-diffraction measurements in the laboratory. The lattice constants in the temperature range from 6 to 300 K were determined by synchrotron x-ray diffraction at BL-8B of the Photon Factory, High Energy Accelerator Research Organization (KEK), measured at $\lambda = 0.99925$ Å. The data were refined using the Rietveld method according to the structure indexed to the space group of *Cc* for $x = 0.00$ and *I*4/*mmm* for $x = 0.10$ [31]. Dielectric measurements were performed in the temperature range from 4 to 740 K using the physical property measurement system and a Linkam THMS600 temperature controller, both of which are equipped with an Agilent 4284A precision LCR meter. Raman-scattering measurements were performed in the backscattering geometry. The excitation light produced by an Oxxius LCX-532S-300 solid-state laser was attenuated at 7 mW and focused on the sample using a 5 × objective lens. The scattered light collected by the same lens was analyzed by a Jobin-Yvon HR320 spectrograph equipped with an Andor iDus420 CCD camera, where the elastic stray component was suppressed using three OptiGrate ultra-narrow-band holographic notch filters.

III. RESULTS AND DISCUSSION

Figure 2 depicts *in situ* crystallization of the Bi-Si-O ternary glass observed by x-ray-diffraction measurements as a function of temperature on heating from 300 to 700 °C, where the bottom panels indicate the calculated diffraction patterns of

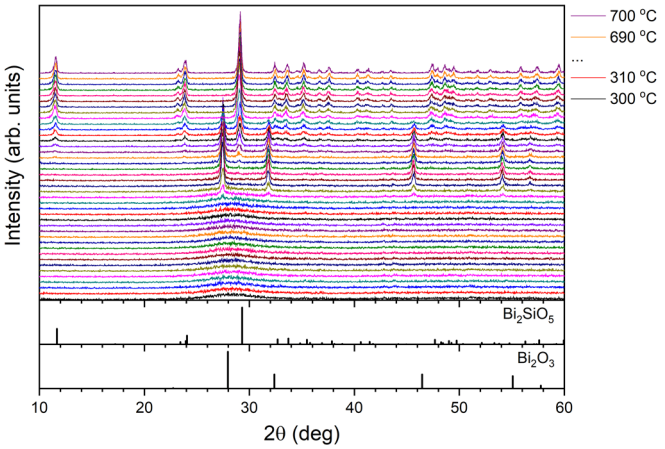

FIG. 2. The crystallization process of Bi-Si-O glass, as observed by *in situ* x-ray-diffraction measurements on heating from 300 to 700 °C. Bottom panels indicate calculated diffraction patterns for Bi_2SiO_5 and Bi_2O_3.

Bi_2SiO_5 and Bi_2O_3. The observed diffraction patterns are aligned with a constant interval of 10 °C. In this paper, we found a two-step crystallization process of the Bi-Si-O glass, as depicted in this figure as well. At 300 °C, a broad diffraction component is seen at around 28 °, indicating the amorphous state of the sample. As temperature elevates, peaks appear at 470 °C and rapidly grow on heating. The observed diffraction pattern is similar to that for Bi_2O_3, although each peak appears in a slightly lower angle from the corresponding calculated position, suggesting that Bi_2O_3 crystals first precipitate in the amorphous matrix. Subsequently, from 540 °C the diffraction pattern gradually overlaps with that for Bi_2SiO_5 and the crossover finishes at approximately 600 °C to indicate completion of the crystallization. Judging from the observed peaks being unchanged on further heating, the crystallized Bi_2SiO_5 is found to be stable at least until 700 °C.

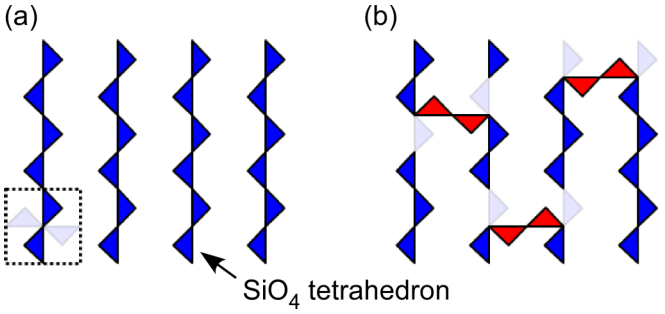

FIG. 4. Schematic for (a) the ordered and (b) the disordered SiO_4 one-dimensional chains. The broken square indicates possible orientations of the SiO_4 tetrahedron.

Powder x-ray-diffraction patterns for the crystallized $(Bi_{1-x}La_x)_2SiO_5$ ($x = 0.00$, 0.01, 0.03, 0.05, 0.07, and 0.10) are presented in Fig. 3 with the calculated pattern for $x = 0.00$ indicated in the bottom panel. While roughly similar patterns are seen for all samples, details systematically change due to the La substitution, as separately indicated in panel (b) on a magnified scale. As shown in Fig. 3(b), a new diffraction peak grows with increasing x in-between two peaks at 32.7 and 33.7 ° that originally exist in pure Bi_2SiO_5. According to the previous study on $(Bi_{1-x}La_x)_2SiO_5$, the newly appeared peak is a sign of disordering of the SiO_4 one-dimensional chains, as illustrated in Fig. 4 [30]. As illustrated in the same figure, the SiO_4 tetrahedra form parallel aligned one-dimensional chains in the original structure of Bi_2SiO_5. The one-dimensional chains are constructed by a pair of corner-linked tetrahedra, which assume specific orientations over several nonequivalent ones, as indicated within the broken square in Fig. 4(b). When the SiO_4-tetrahedra form the one-dimensional chains with complete ordering, the 020_M and 002_M diffraction peaks are observed due to in-plane anisotropy, as presented in Fig. 3(b) for $x = 0.00$, where the subscript "M" denotes the monoclinic phase. If disordering of the SiO_4 tetrahedra takes place in

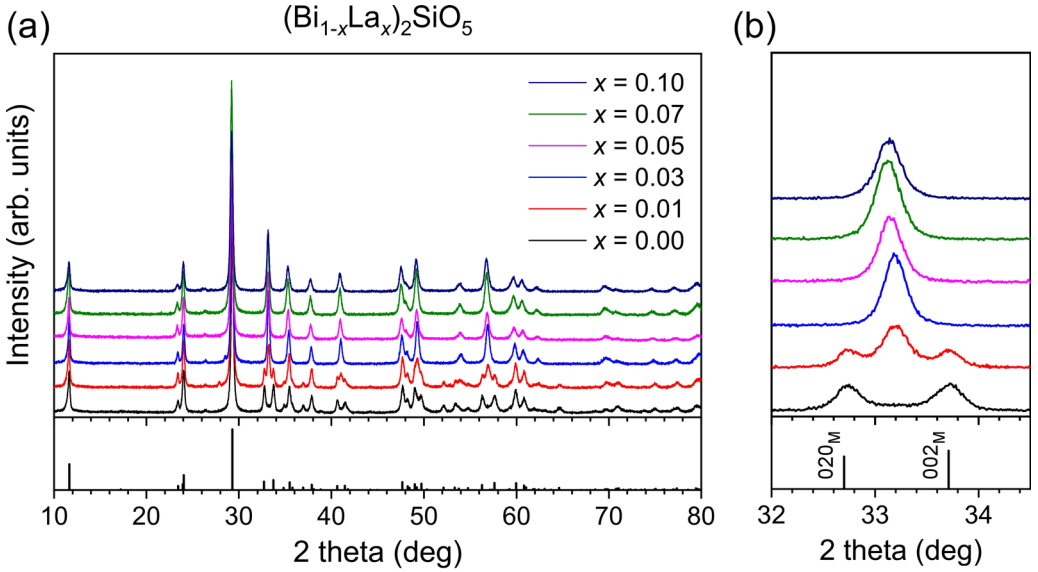

FIG. 3. (a) Powder-diffraction patterns of $(Bi_{1-x}La_x)_2SiO_5$ observed at room temperature, where baselines are systematically offset. The bottom panel indicates a calculated pattern for pure Bi_2SiO_5. (b) A magnified graph of the diffraction patterns for a range from 32.0 to 34.5 °.

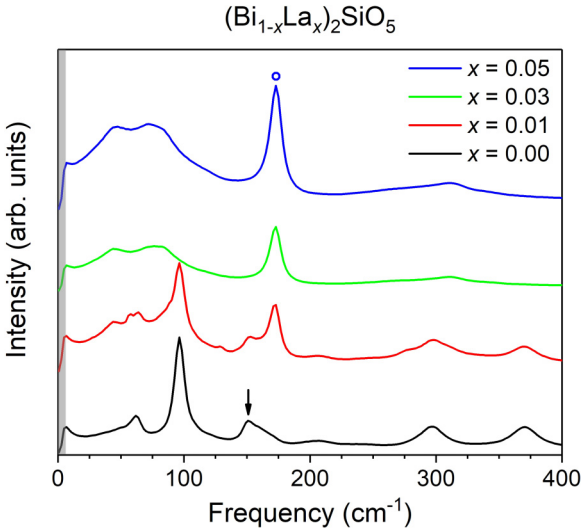

FIG. 5. Raman-scattering spectra of $(Bi_{1-x}La_x)_2SiO_5$ ($x = 0.00$, 0.01, 0.03, and 0.05). The arrow and the circle in the figure denote the peaks that characterize the spectra for $x = 0.00$ and 0.05.

a sufficiently large area, over which the anisotropy is lost as an average structure, the 020_M and 002_M peaks partially merge to a single diffraction peak that appears between the original peaks. Note here that the diffraction peaks are indexed in terms of the monoclinic phase. In $(Bi_{1-x}La_x)_2SiO_5$ with $x = 0.01$, as shown in the same figure, the single peak at around 33° superposes the pair of 020_M and 002_M peaks, indicating coexistence of ordered and disordered chains in the matrix. Additionally, on further introduction of La, only the merged single peak remains, demonstrating that the one-dimensional chains are completely disordered and the crystal structure becomes macroscopically tetragonal.

Figure 5 presents the Raman-scattering spectra of $(Bi_{1-x}La_x)_2SiO_5$ ($x = 0.00$, 0.01, 0.03, and 0.05). The Raman spectrum of $(Bi_{1-x}La_x)_2SiO_5$ drastically changes with respect to the number of peaks and their positions as x increases. This implies that lattice dynamics is markedly modified by the La substitutions. Especially, the spectrum profile becomes discontinuously smooth for x larger than 0.03.

Focused on the characteristic spectral peaks in the samples with $x = 0.00$ and 0.05, which are, respectively, indicated by the arrow and the circle in Fig. 5, $(Bi_{1-x}La_x)_2SiO_5$ ($x = 0.01$) can be understood as superposition of the spectra for $x = 0.00$ and 0.05. This confirms the phase coexistence suggested by the x-ray-diffraction measurements. Judging from the spectrum for $x = 0.01$, which involves peaks for $x = 0.00$ and 0.05 without significant peak shifts, both phases seem to be independent.

Temperature dependences of dielectric permittivity and tanδ measured in $(Bi_{1-x}La_x)_2SiO_5$ ($x = 0.00$, 0.01, 0.03, 0.05, 0.07, and 0.10) over a temperature range from 2 to 760 K are plotted as a function of temperature in Figs. 6(a) and 6(b), respectively. Indicated by an open square in panel (a), the permittivity of $(Bi_{1-x}La_x)_2SiO_5$ with $x = 0.00$ shows a sharp peak at 710 K, suggesting the occurrence of ferroelectric phase transition from the orthorhombic *Cmcm* phase to the monoclinic *Cc* phase on cooling. Note here that the observed transition temperature for $(Bi_{1-x}La_x)_2SiO_5$ with $x = 0.00$ is slightly higher than that reported in previous studies [23,32]. This discrepancy might be due to a difference in the synthesis method. On the La substitution with $x = 0.01$, the phase transition temperature decreases to 670 K and the dielectric peak becomes broadened. On further increment of La content x, the dielectric peak immediately vanishes owing to the disappearance of the ferroelectricity. If the La substitution systematically suppresses the ferroelectric interaction of $(Bi_{1-x}La_x)_2SiO_5$ the phase transition temperature is expected to continuously fall into 0 K as x increases. Such immediate disappearance of the phase transition is explained below; namely, the ordered tetrahedral chain is chemically unstable with La, and thereby a different $(Bi_{1-x}La_x)_2SiO_5$ phase with disordered tetrahedra

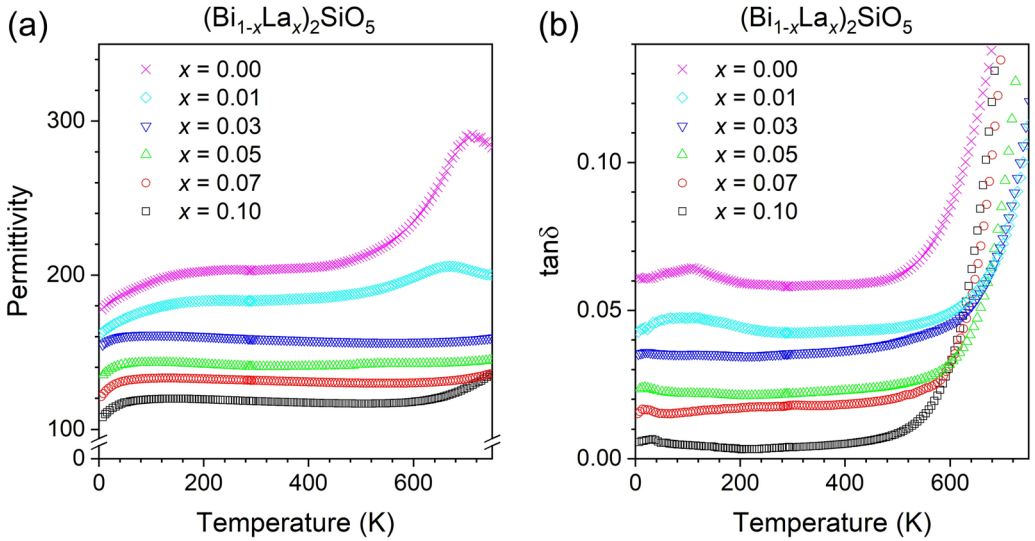

FIG. 6. Temperature dependences of (a) dielectric permittivity and (b) tanδ for $(Bi_{1-x}La_x)_2SiO_5$ ($x = 0.00$, 0.01, 0.03, 0.05, 0.07, and 0.10) ceramics observed at 100 kHz over the temperature range from 2 to 760 K. The data plots $x = 0.01$, 0.03, 0.05, 0.07, and 0.10 are, respectively, shifted for the sake of visibility.

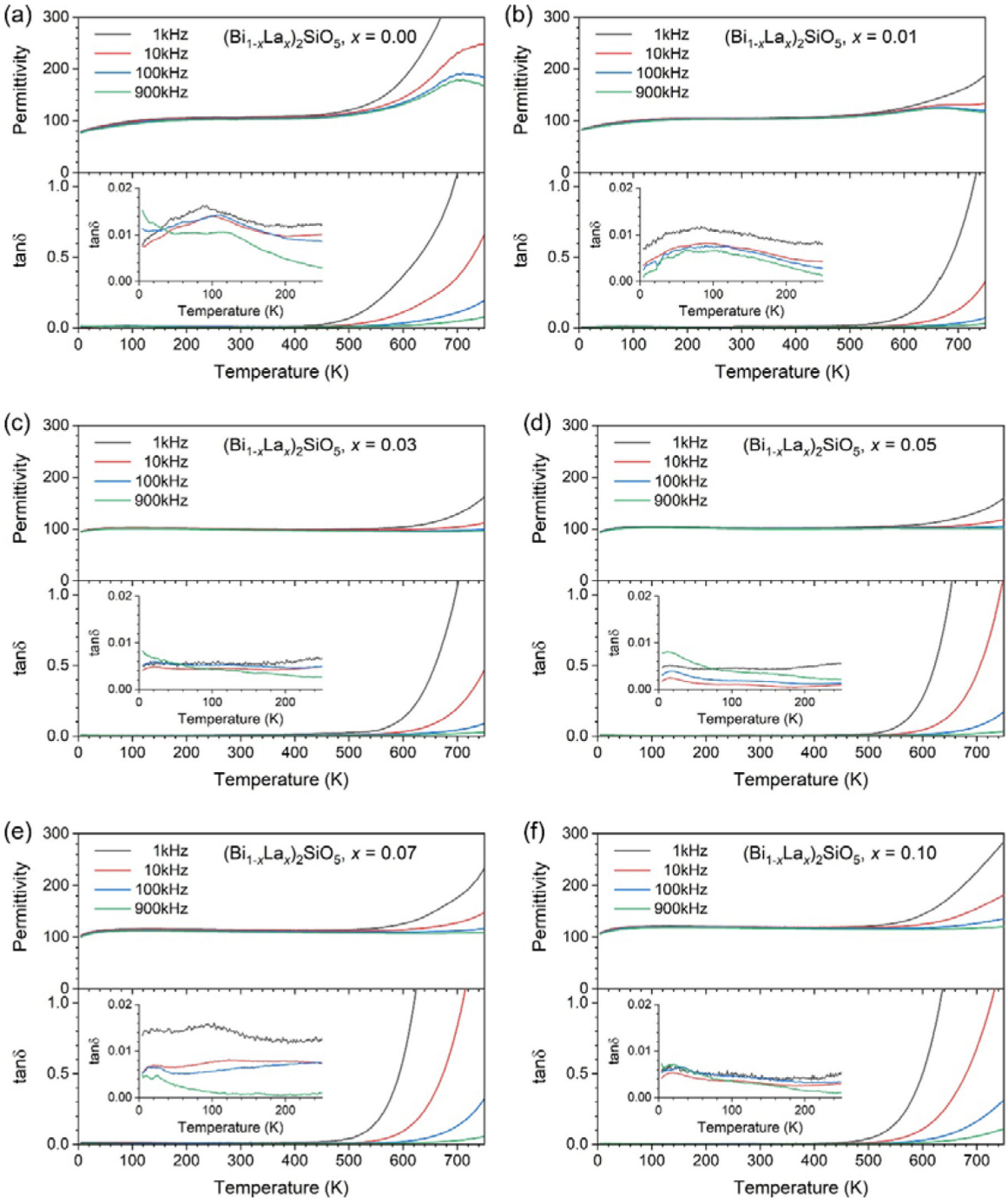

FIG. 7. Temperature dependence of dielectric permittivity and tanδ for $(Bi_{1-x}La_x)_2SiO_5$ observed with several test frequencies. The inset in each panel presents temperature variation of tanδ from 0 to 250 K with magnified scale.

may exist at the high La-content region, with which the original $(Bi_{1-x}La_x)_2SiO_5$ phase with the ordered tetrahedra has limited solid solubility. This observation is consistent with the phase coexistence state clarified by the powder x-ray-diffraction and Raman-scattering measurements. The results observed in $(Bi_{1-x}La_x)_2SiO_5$ are in marked contrast to the case for the Pb-substituted Bi_2SiO_5, $(Bi_{1-x}Pb_x)_2SiO_5$, where the ordered tetrahedra still survive even until $x = 0.2$ to maintain ferroelectricity in spite of dense oxygen vacancies due to the heterovalent substitution of Bi^{3+} with Pb^{2+} [32]. Considering that $(Bi_{1-x}La_x)_2SiO_5$ ferroelectricity also persists within the composition range where the one-dimensional SiO_4 chains remain, the stereochemical activity of the Bi-site ion supports SiO_4-tetrahedra ordering, giving rise to ferroelectricity in Bi_2SiO_5. Additionally, in the composition range with $x > 0.03$, where the ferroelectricity is completely suppressed, dielectric permittivity shows a flat temperature variation with a rather high permittivity of approximately 100 over a wide temperature range. The gradual increase of permittivity in the high-temperature region, which is particularly prominent in $x = 0.10$, stems from increase in conductivity as indicated by the sharp enhancement of tanδ presented in panel (b). The

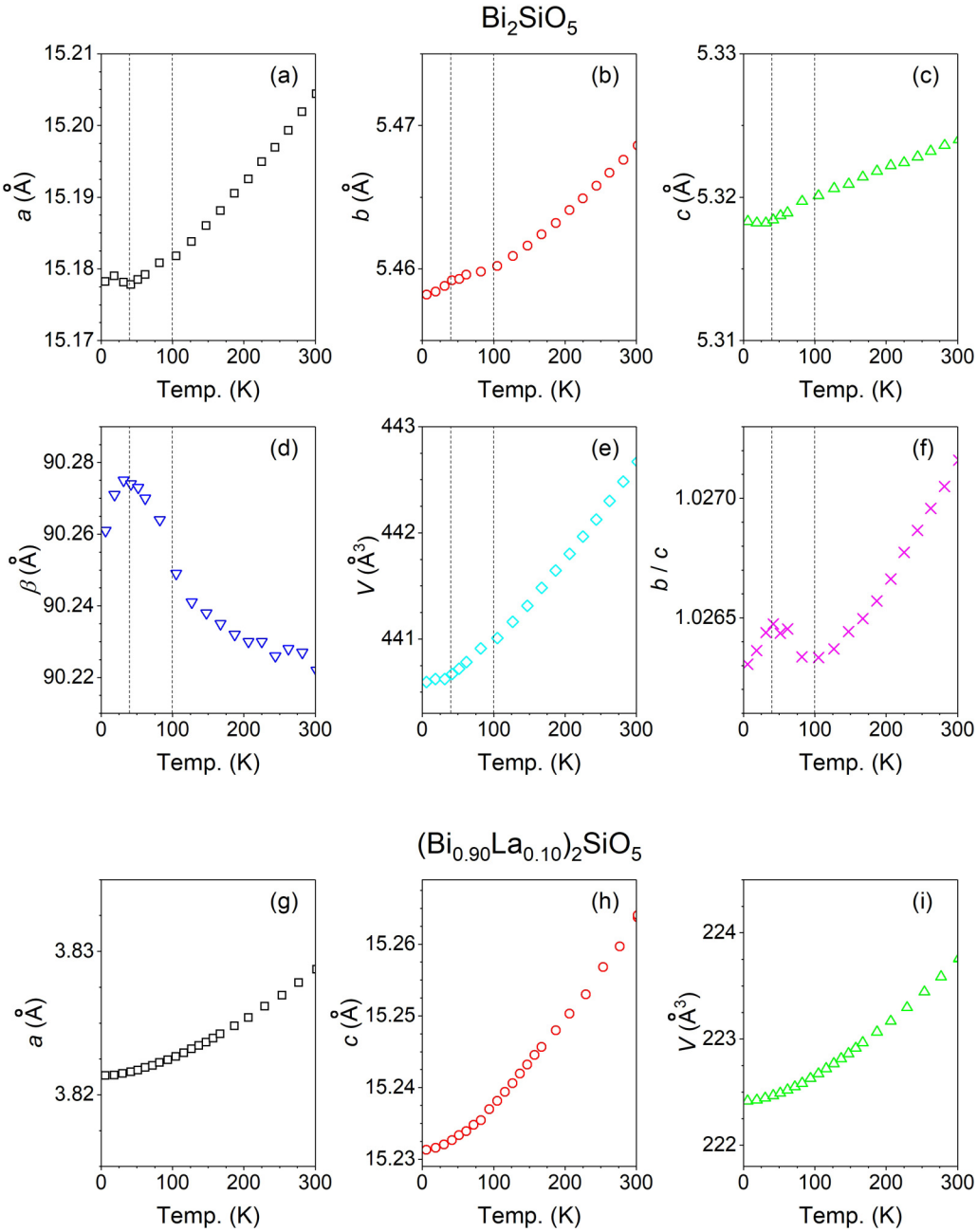

FIG. 8. Temperature dependences of lattice parameters for $(Bi_{1-x}La_x)_2SiO_5$ with $x = 0.00$ and 0.10. For $x = 0.00$ with the monoclinic symmetry, the lattice parameters a, b, c, and β are plotted in the panels (a), (b), (c), and (d), respectively. The lattice volume V and the in-plane anisotropy parameter b/c are, respectively, presented in panels (e) and (f). For $x = 0.10$ with tetragonal symmetry, on the other hand, the lattice parameters a and c and the volume V are plotted in panels (g), (h), and (i), respectively.

tanδ in the high-temperature region is markedly enhanced by decreasing the test frequency as presented in Fig. 7.

A dielectric anomaly in the low-temperature region of $(Bi_{1-x}La_x)_2SiO_5$ with $x = 0.00$ and 0.01 is an unexpected discovery. In $(Bi_{1-x}La_x)_2SiO_5$ with $x = 0.00$ and 0.01 [as presented in Fig. 6(a)] the dielectric permittivity shows a steep decline in the low-temperature region below 100 K. Synchronized with an onset of the declination, tanδ exhibits a peaklike anomaly [Fig. 6(b)]. These behaviors strongly indicate that an additional phase transition takes place in the ferroelectric phase. In $(Bi_{1-x}La_x)_2SiO_5$ with $x = 0.00$, the peaklike anomaly in tanδ shows frequency dispersion as presented in Fig. 7(a), manifesting the diffuse characteristic of the additional phase transition. We examined temperature dependences of the lattice parameters in detail to investigate an origin of the dielectric anomaly in the low-temperature region of $(Bi_{1-x}La_x)_2SiO_5$ with $x = 0.00$ and 0.01 that has been found in this paper. The temperature dependences of the lattice parameters a, b, and c and the monoclinic angle β of the ferroelectric phase of $(Bi_{1-x}La_x)_2SiO_5$ at $x = 0.00$ with monoclinic Cc symmetry are presented in Figs. 8(a)–8(d). The lattice volume V and an in-plane asymmetry parameter

b/*c* are also plotted in Figs. 8(e) and 8(f), respectively. As indicated by dotted lines in panels (a)–(c), two anomalies are detected for every crystallographic axis in addition to an ordinary thermal contraction. The anomalies are more distinct in the monoclinic angle and the in-plane anisotropy parameter as plotted in panels (d) and (f), but they are obscure in the lattice volume plotted in panel (e). Out of the two observed anomalies, the higher-temperature one is in good agreement with the dielectric anomaly in terms of the temperature where it appears. Though it is not clear why no corresponding dielectric anomaly was detected for the other lattice anomaly at the lower temperature, the present experiments at least confirm that the observed dielectric anomaly is certainly accompanied by lattice distortions. Since no extra peaks and/or additional peak splitting appeared in the x-ray-diffraction patterns on cooling to the lowest temperature, a further symmetry reduction from the monoclinic *Cc* can be ruled out within the accuracy of the present experiments. A possible origin for the low-temperature dielectric anomaly would thus be an isosymmetric phase transition, which has been theoretically proposed and experimentally demonstrated in several compounds including multiferroics and superconductors [33–39]. In $(Bi_{1-x}La_x)_2SiO_5$ with $x = 0.01$, the low-temperature anomaly slightly shifts to a lower temperature, and the peak of tanδ broadens. With further increase of the La content x, the peak of tanδ completely disappears, being consistent with the results shown in Figs. 8(g)–8(i) where the low-temperature lattice anomaly also disappears. This trend is in excellent agreement with the x dependence of ferroelectricity discussed above. Note that the weak drop of permittivity in the lowest temperature for $(Bi_{1-x}La_x)_2SiO_5$ with $x \geqslant 0.03$ might be a trace of the dielectric anomaly due to partial ordering of SiO_4 remaining in the disordered matrix. Considering that the ferroelectricity of $(Bi_{1-x}La_x)_2SiO_5$ is driven by the twisting of one-dimensional SiO_4 chains, the observed synchronization between ferroelectricity and low-temperature anomaly disappearances suggests that the origin of the low-temperature anomaly is closely linked to the ordered one-dimensional SiO_4 chains. In fact, a recent study by Ohi *et al.* clarified the reversible isosymmetric phase transition in orthopyroxene, which possesses one-dimensional SiO_4-tetrahedral chains in the crystal structure similar to Bi_2SiO_5 [40]. Since the isosymmetric phase transition should be of the first order, a heat capacity measurement would provide crucial information to clarify whether the observed low-temperature anomaly stems from the isosymmetric phase transition or not.

IV. CONCLUSION

The isovalent La-substitution effect on the crystal structure and ferroelectricity of Bi_2SiO_5 was examined in this paper. Systematic experiments with x-ray-diffraction and Raman-scattering measurements on $(Bi_{1-x}La_x)_2SiO_5$ ceramics, which were synthesized by the crystallization of Bi-Si-O and Bi-La-Si-O stoichiometric glasses, have clarified the occurrence of disordering in the one-dimensional chains of SiO_4 tetrahedra in the composition range of $x \geqslant 0.03$. Dielectric measurements have demonstrated that the ferroelectricity of $(Bi_{1-x}La_x)_2SiO_5$ disappears in association with disordering of the SiO_4 chains, confirming that these SiO_4 chains play a crucial role in the ferroelectricity of Bi_2SiO_5. Compared to the heterovalent substitution of Pb^{2+} for Bi^{3+}, the isovalent La^{3+} substitution has been found to much more seriously perturb the ordering of SiO_4 tetrahedra than Pb^{2+}, indicating the importance of the stereochemical activity of lone-pair electrons for the ferroelectricity of Bi_2SiO_5. Lastly, distinct signs of the additional phase transition in the ferroelectric phase of Bi_2SiO_5 have been found in this paper. Since no trace of symmetry change was detected within the present experimental accuracy, the additional transition is the isosymmetric phase transition that has been reported in pyroxenes, which are also composed of one-dimensional SiO_4 chains [40].

ACKNOWLEDGMENTS

This paper is partially supported by a Grant-in-Aid for Young Scientists (A) (Grant No.16H06115) and a Ministry of Education, Culture, Sports, Science and Technology Element Strategy Initiative Project to Form Core Research Center. The authors thank Dr. Yuki Sakai and Prof. Masaki Azuma for preliminary x-ray-diffraction measurements, and Prof. Mitsuru Itoh for fruitful discussion. The synchrotron x-ray-diffraction study was performed with the approval of the Photon Factory Program Advisory Committee (Grant No. 2016S2-004).

[1] M. E. Lines and A. M. Glass, *Principles and Applications of Ferroelectrics and Related Materials* (Clarendon, Oxford, 1977).
[2] G. H. Haertling, J. Am. Ceram. Soc. **82**, 797 (1999).
[3] I. B. Bersuker, Phys. Rev. Lett. **108**, 137202 (2012).
[4] R. G. Pearson, J. Am. Chem. Soc. **91**, 4947 (1969).
[5] R. G. Pearson, J. Mol. Struct. (THEOCHEM) **103**, 25 (1983).
[6] T. Hughbanks, J. Am. Chem. Soc. **107**, 6851 (1985).
[7] R. A. Wheeler, M. H. Whangbo, T. Hughbanks, R. Hoffmann, J. K. Burdett, and T. A. Albright, J. Am. Chem. Soc. **108**, 2222 (1986).
[8] M. Kunz and I. D. Brown, J. Solid State Chem. **115**, 395 (1995).
[9] J. B. Goodenough, Annu. Rev. Mater. Sci. **28**, 1 (1998).
[10] R. Seshadri and N. A. Hill, Chem. Mater. **13**, 2892 (2001).
[11] P. S. Halasyamani, Chem. Mater. **16**, 3586 (2004).
[12] K. A. Müller and H. Burkard, Phys. Rev. B **19**, 3593 (1979).
[13] W. Kleemann, J. Dec, and B. Westwański, Phys. Rev. B **58**, 8985 (1998)
[14] M. Itoh, R. Wang, Y. Inaguma, T. Yamaguchi, Y-J. Shan, and T. Nakamura, Phys. Rev. Lett. **82**, 3540 (1999).
[15] H. Taniguchi, M. Itoh, and T. Yagi, Phys. Rev. Lett. **99**, 017602 (2007).
[16] V. Westphal, W. Kleemann, and M. D. Glinchuk, Phys. Rev. Lett. **68**, 847 (1992).
[17] B. E. Vugmeister, Phys. Rev. B **73**, 174117 (2006).
[18] I. Grinberg, P. Juhas, P. K. Davies, and A. M. Rappe, Phys. Rev. Lett. **99**, 267603 (2007).
[19] D. Fu, H. Taniguchi, M. Itoh, S. Y. Koshihara, N. Yamamoto, and S. Mori, Phys. Rev. Lett. **103**, 207601 (2009).
[20] R. E. Cohen, Nature (London) **358**, 136 (1992).

[21] N. A. Benedek and C. J. Fennie, Phys. Rev. Lett. **106**, 107204 (2011).
[22] M. Ye and D. Vanderbilt, Phys. Rev. B **93**, 134303 (2016).
[23] H. Taniguchi, A. Kuwabara, J Kim, Y Kim, H. Moriwake, S. Kim, T. Hoshiyama, T. Koyama, S Mori, M. Takata, H. Hosono, Y. Inaguma, and M. Itoh, Angew. Chem. Int. Ed. **52**, 8088 (2013).
[24] Y. Kim, J. Kim, A. Fujiwara, H. Taniguchi, S. Kim, H. Tanaka, K. Sugimoto, K. Kato, M. Itoh, H. Hosono, and M. Takata, IUCrJ **1**, 160 (2014).
[25] D. Seol, H. Taniguchi, J. Hwang, M. Itoh, H. Shin, S. W. Kim, and Y. Kim, Nanoscale **7**, 11561 (2015).
[26] J. Park, B. G. Kim, S. Mori, and T. Oguchi, J. Solid State Chem. **235**, 68 (2016).
[27] N. Setter, M. E. Mendoza-Alvarez, W. Depmeier, and H. Schmid, Ferroelectrics **56**, 49 (1984).
[28] Y. Maeda, T. Wakamatsu, A. Konishi, H. Moriwake, C. Moriyoshi, Y. Kuroiwa, K. Tanabe, I. Terasaki, and H. Taniguchi, Phys. Rev. Applied **7**, 034012 (2017).
[29] T. Wakamatsu, K. Tanabe, I. Terasaki, and H. Taniguchi, Phys. Status Solidi RRL **11**, 1700009 (2017).
[30] S. Georges, F. Goutenoire, and P. Lacorre, J. Solid State Chem. **179**, 4020 (2006).
[31] F. Izumi and K. Momma, Solid State Phenom. **130**, 15 (2007).
[32] H. Taniguchi, T. Nakane, T. Nagai, C. Moriyoshi, Y. Kuroiwa, A. Kuwabara, M. Mizumaki, K. Nitta, R. Okazaki, and Ichiro Terasaki, J. Mater. Chem. C **4**, 3168 (2016).
[33] R. A. Cowley, Phys. Rev. B **13**, 4877 (1976).
[34] K. Aizu, J. Phys. Soc. Jpn. **54**, 203 (1985).
[35] A. G. Christy, Acta Crystallogr. Sect. B **51**, 753 (1995).
[36] H. Kiriyama, K. Kitahara, O. Nakamura, and R. Kiriyama, Bull. Chem. Soc. Jpn. **46**, 1389 (1973).
[37] J. F. Scott, Adv. Mater. **22**, 2106 (2010).
[38] J. Yamaura, M. Takigawa, O. Yamamuro, and Z. Hiroi, J. Phys. Soc. Jpn. **79**, 043601 (2010)
[39] S. Bhattacharjee, K. Taji, C. Moriyoshi, Y. Kuroiwa, and D. Pandey, Phys. Rev. B **84**, 104116 (2011).
[40] S. Ohi, A. Miyake, N. Shimobayashi, M. Yashima, and M. Kitamura, Am. Mineral. **93**, 1682 (2008).